Available online at www.sciencedirect.com

ScienceDirect

Journal of the Franklin Institute 360 (2023) 4071–4090

www.elsevier.com/locate/jfranklin

Four-dimensional indoor visible light positioning: A deep-learning-based perspective

Danping Su[a], Xianyao Wang[a], Sicong Liu[a,b,*], Wenbo Ding[c]

[a] *School of Informatics, Xiamen University, Xiamen 361005, China*

[b] *National Mobile Communications Research Laboratory, Southeast University, Nanjing 210096, China*

[c] *Tsinghua-Berkeley Shenzhen Institute, Tsinghua Shenzhen International Graduate School, Tsinghua University, Shenzhen 518055, China*

Received 29 September 2022; received in revised form 14 December 2022; accepted 5 February 2023
Available online 16 February 2023

Abstract

Accurate indoor positioning has been a difficult problem as the *last meter* dilemma of localization and navigation due to lack of satellite navigation signals and complex characteristics of multipath and dynamic indoor channels. Indoor visible light positioning (VLP) provides a new possible paradigm for accurate and low-complexity indoor positioning using widely deployed light-emitting diodes (LED). In this paper, the received signal strength of the photodetector at a mobile terminal is utilized to extract the geometric features in order to infer the accurate position coordinate via deep learning. Specifically, a hybrid model, i.e., a convolutional-recurrent neural network (CRNN), is devised to learn the nonlinear mapping from the received signal strength to the position coordinates in the complex indoor visible light propagation environment. A four-dimensional (4D) VLP architecture based on CRNN is formulated to deal with the non-line-of-sight propagation of indoor visible light and different receiver orientation. Simulation results show that the proposed CRNN-based 4D VLP (CR4D-VLP) method can achieve centimeter-level positioning accuracy, and significantly outperforms other state-of-the-art deep-learning-based schemes in both line-of-sight and non-line-of-sight scenarios with various spatial patterns of LEDs and different room sizes.

* Corresponding author at: School of Informatics, Xiamen University, Xiamen 361005, China.

E-mail addresses: sudanping@stu.xmu.edu.cn (D. Su), 23320211154197@stu.xmu.edu.cn (X. Wang), liusc@xmu.edu.cn (S. Liu), ding.wenbo@sz.tsinghua.edu.cn (W. Ding).

https://doi.org/10.1016/j.jfranklin.2023.02.015

1. Introduction

The rapid development of positioning and navigation technologies has provided a wealth of location based services (LBS) [1]. However, satellite positioning systems such as the global positioning system (GPS) that performs well outdoors do not work for indoor positioning due to signal blockage [2]. It is necessary to study effective techniques for accurate indoor positioning. Currently, indoor localization methods based on Wi-Fi [3], radio frequency identification (RFID) [4], Bluetooth [5], ultra-wideband (UWB) [6] and other wireless communication technologies have emerged.

Recently, visible light communication (VLC) utilizing LEDs has drawn great attention from both academia and industry. VLC has a huge unlicensed bandwidth and is naturally energy efficient. VLC is also suitable for special scenarios sensitive to electromagnetic pollution, such as hospitals and airplanes [7–10]. Thus, indoor visible light positioning (VLP) implemented based on the VLC technique has emerged as a promising alternative for indoor localization [11].

Classical radio-frequency-based wireless positioning methods roughly include two categories. One category is based on the ranging information conveyed by the signals, such as received signal strength (RSS) [12], angle of arrival (AoA) [13], time of arrival (ToA) [14], time difference of arrival (TDoA), and frequency difference of arrival (FDoA) [15,16]. The other category is based on non-ranging information such as Distance Vector Hop algorithm [17], K-nearest neighbor method [18] and fingerprint matching method [19]. However, the accuracy of wireless based positioning methods, such as Wi-Fi, Bluetooth, RFID and UWB, etc., need to be further improved, especially for the LBS with requirements of centimeter-level positioning in scenarios such as industrial internet-of-things and smart manufacturing.

As a prospective high-precision indoor localization approach, VLP has been investigated in literature [20–27]. In [20], a nonlinear optimization model based on graph optimization was proposed to process the RSS data for VLP, and the experimental results showed that the proposed model significantly improves the positioning accuracy. An algorithm based on the maximum likelihood principle was proposed in Steendam [21] to estimate the AoA and obtain the position of the receiver, which can achieve centimeter-level performance. However, the performance of conventional VLP methods still need to be improved, especially in complex indoor scenarios such as complex LED patterns, non-line-of-sight (NLOS) propagation, dynamic channels, and in case of different user terminal orientation.

Deep learning has achieved great success in many areas such as computer vision and natural language processing [28,29]. There have been some studies incorporating deep learning into localization [30–33]. In [34], an indoor VLP technique using deep neural network (DNN) based on Bayesian regularization with sparse training point was proposed, which provided a new solution for real-time and high-accuracy positioning. In [35], a passive indoor VLP system assisted by deep learning was proposed and the experimental results demonstrated that the localization performance was related to the signal-to-noise ratio (SNR) and the size of training datasets. A VLP method based on multiple photodiodes (PD) and machine learning was proposed in Bakar et al. [36], which can reduce the time and implementation complexity. However, the challenges of complex conditions of NLOS propagation and different receiver rotation remain to be addressed.

In this paper, an indoor VLP method based on deep learning is proposed, in which the geometric information is extracted from the RSS at the PD of the user terminal by deep learning models. To better extract the features, a hybrid deep learning model, i.e., a convolutional-

recurrent neural network (CRNN), is devised. To tackle the problem of dynamically changing orientation of the user terminal, a CRNN-based four-dimensional VLP (CR4D-VLP) framework is formulated, which accounts for both the three-dimensional (3D) spatial coordinates and the user terminal orientation as the fourth dimension via coordinate rotation. Moreover, the realistic complex NLOS propagation of the visible light is taken into consideration in the design of the proposed CR4D-VLP method. The positioning performance in conditions of various LED spatial patterns and different room sizes is investigated via simulations. The theoretical bound of the positioning accuracy is derived. The contributions of this paper are summarized as follows:

- A 4D indoor VLP framework is formulated, in which the user terminal orientation is taken into account utilizing coordinate rotation.
- A hybrid CRNN-based deep learning model is devised to learn the inherent geometric feature from the RSS data acquired in a complex and dynamic indoor environment.
- The realistic complex NLOS propagation characteristics of the indoor visible light signals are exploited for accurate 4D positioning.

The remainder of the paper is organized as follows: Related works are surveyed in Section 2. The system model is described in Section 3. In Section 4, the proposed CR4D-VLP method is introduced and the theoretical bound is derived. Simulation results are reported and discussed on in Section 5, followed by the concluding remarks in Section 6.

2. Related works

2.1. Radio-frequency-based indoor localization techniques

Many radio-frequency-based indoor localization techniques have been presented [3–6,37–40] over the recent years.

A frequency hopping approach was proposed in Chen et al. [3] to achieve centimeter-level accuracy indoor localization on Wi-Fi platforms. Ma et al. [4] proposed a weighted multidimensional scaling method in a tag-to-tag communication system to conduct multi-tag indoor cooperative localization, where the targets were marked with passive ultrahigh frequency RFID tags. In [5], a precise dead reckoning algorithm based on Bluetooth and multiple sensors was proposed for indoor localization and the experiment results showed that the algorithm improved the positioning accuracy and applicability. A novel localization framework was presented based on UWB channel sounding in Xu et al. [6] which can achieve an average accuracy of 0.26, 0.28 and 0.90 m in line-of-sight (LOS) obstructed-LOS, and NLOS scenarios, respectively. Wang et al. [37] developed an RFID-based localization system based on RFID tags in indoor scenarios. A Wi-Fi-based localization system was proposed to improve the accuracy of fingerprint-based indoor localization in Sun et al. [38]. Hanssens et al. [39] presented a fixed-lag extended finite impulse response smoother algorithm based on the distance between the UWB reference nodes and a blind node, and extensive experiments demonstrated that it had higher accuracy and robustness. In [40], an ensemble model consisting of fuzzy classifier and multi-layer perceptron for indoor Wi-Fi-based parking localization was proposed to achieve higher accuracy and lower error.

2.2. Visible-light-based indoor localization techniques

2.2.1. Conventional VLP schemes

There are plenty of conventional VLC-based indoor localization approaches in literature. By detecting the phase difference between the transmitted signals, TDoA was estimated to realize VLC-based localization in Jung et al. [22]. Du et al. [23] developed a low-complexity TDoA-based indoor VLP system using an enhanced practical localization scheme based on cross correlation. Chen et al. [24] analyzed the potential of code division multiple access (CDMA)-based indoor VLP. An algorithm based on the maximum likelihood principle was proposed in Steendam [21] to estimate the AoA and obtain the position of the receiver, which can achieve centimeter-level performance. In [25], a 3D indoor VLP algorithm based on the AoA and RSS was proposed, which can obtain the estimated position with less than 6 cm. Zhu et al. [26] proposed an indoor VLP framework based on the angle differences of arrival. In [27], the hybrid utilization of the AoA and RSS information was proposed in VLC systems for 3D localization.

2.2.2. Learning-based VLP schemes

Recently, some studies applying artificial intelligence into VLC-based indoor localization have emerged in literature [34–36,41–48]. In [41], an artificial neural-network-based VLP algorithm was proposed in a diffuse channel. Guo et al. [42] proposed several representative machine learning algorithms to train multiple classifiers based on RSS fingerprints and presented two robust fusion localization algorithms to combine the outputs of these classifiers. Liu et al. [43] proposed an indoor VLP algorithm based on machine learning considering the indoor reflection of the visible light and presented a hybrid positioning algorithm based on extreme learning machine and the density-based spatial clustering to improve localization accuracy. Hong et al. put forward an AoA-based VLP system using quadrant-solar-cell and third-order ridge regression machine learning to improve the localization accuracy in Hong et al. [44]. A neural network algorithm was proposed to correct the error caused by the tilt angle of the camera in VLP system in Yuan et al. [45] and the experimental results indicated that it can achieve high-precision positioning.

In [46], a novel position estimation DNN was proposed to address the issues of weak compatibility and high complexity of VLP. A VLP system based on RSS was proposed in Hsu et al. [47] which utilized data pre-processing and convolutional neural networks (CNN) to address the issue of light deficient regions in VLP system. Lin et al. [48] proposed a positioning scheme based on unit cell model duplication and devised a residual concatenation neural network utilizing transfer learning to refine the model of the target positioning unit cell to enhance the positioning accuracy of VLP.

3. System model

3.1. Indoor visible light positioning model

As shown in Fig. 1, let us consider the indoor VLP problem in a room whose length, width and height are $L \times W \times H$, where a Cartesian coordinate system is established.

In the room, a certain number of LEDs are deployed with equal spacing on the ceiling and a user terminal equipped with a PD can move randomly in a 3D space with size of $l \times w \times h$. Specifically, the user terminal can also rotate its receive plane in any angle. The PD of the

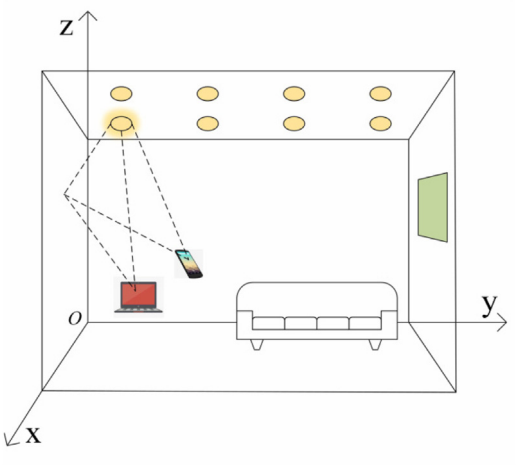

Fig. 1. The indoor VLC localization scenario.

user terminal receives information conveyed by the visible light signals sent from the LEDs. Using this coordinate system, the coordinates and the geometrical relationships between the LEDs and the PD can be explicitly represented.

3.2. Visible light propagation channel

The LED radiates the same light intensity to any angle, which conforms to Lambert's law [49]. Specifically, the LED source can be regarded as a generalized Lambertian radiation source, and its radiation intensity can be expressed as

$$R(\theta) = \frac{(m+1)}{2\pi}\cos^m(\theta) \quad -\frac{\pi}{2} \leqslant \theta \leqslant \frac{\pi}{2}, \tag{1}$$

where θ is the irradiation angle of the LED and m is called the Lambertian radiation ordinal whose value is related to the intensity of a half-power angle of the LED. The relationship between θ and m can be described as $m = -\ln 2/\ln\left(\cos\theta_{1/2}\right)$, where $\theta_{1/2}$ is the half-power angle.

As shown in Fig. 2, when the visible light passes through the free space indoors, the DC gain of the LOS channel can be expressed as

$$H_L(0) = \begin{cases} \frac{(m+1)A_{\mathrm{PD}}}{2\pi d^2}\cos^m(\theta)\cos(\phi)T_s(\phi)g(\phi) & 0 \leqslant \phi \leqslant \phi_{\mathrm{FOV}} \\ 0 & \text{otherwise} \end{cases}, \tag{2}$$

where ϕ is the angle of incidence at the PD, d is the distance between the LED and the PD, ϕ_{FOV} is the field of view (FOV) of the PD, A_{PD} is the effective area of the PD, $T_s(\phi)$ is the gain of the optical filter, and $g(\phi)$ is the gain of the optical concentrator defined as

$$g(\phi) = \begin{cases} \frac{n^2}{\sin^2\phi_{\mathrm{FOV}}} & 0 \leqslant \phi \leqslant \phi_{\mathrm{FOV}} \\ 0 & \text{otherwise} \end{cases}, \tag{3}$$

where n is the refractive index of the optical concentrator. Therefore, the received optical power P_r can be obtained by $P_r = R_{\mathrm{PD}}P_tH_L(0)$ when the optical radiation power is P_t. Then

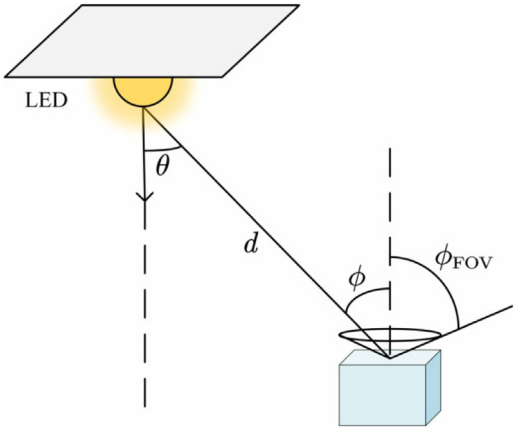

Fig. 2. The LOS propagation of visible light.

the received electrical power can be given by

$$P_{\text{ele}} = [R_{\text{PD}} P_t H_L(0)]^2 + \sigma_n^2, \tag{4}$$

where R_{PD} is the responsivity of the PD, σ_n^2 is the variance of the total noise which mainly includes shot noise and thermal noise, whose variance can respectively be expressed as

$$\sigma_{\text{sh}}^2 = 2qR_{\text{PD}} P_r B + 2qI_{\text{bg}} I_2 B, \tag{5}$$

$$\sigma_{\text{th}}^2 = \frac{8\pi k T_k}{G} \eta A_{\text{PD}} I_2 B^2 + \frac{16\pi^2 k T_k \Gamma}{g_m} \eta^2 A_{\text{PD}}^2 I_3 B^3, \tag{6}$$

where q is the electron charge, B is the equivalent noise bandwidth, I_{bg} is the background noise current, k is the Boltzmann constant, I_2 is the noise bandwidth coefficient, T_k is the thermodynamic temperature, η is the PD capacitance per unit area, G is the open-loop voltage gain, g_m is the FET transconductance coefficient, Γ is the FET channel noise figure, and I_3 is the thermal noise figure.

As shown in Fig. 3, when the visible light reaches an object, reflection will occur, which causes NLOS propagation. The reflection area can be deemed as a virtual visible light source, which can be modeled as Lambertian reflection with satisfactory accuracy [49]. Thus, the DC gain of the NLOS channel in the case of the first reflection can be given by

$$\mathrm{d}H_N(0) = \begin{cases} \frac{(m+1)A_{\text{PD}}}{2\pi d_{11}^2 d_{12}^2} \rho \mathrm{d}A_{\text{ref}} \cos^m(\theta_{11}) \cos(\phi_{11}) \cos(\theta_{12}) T_s(\phi_{12}) g(\phi_{12}) \cos(\phi_{12}) & 0 \leqslant \phi_{12} \leqslant \phi_{\text{FOV}} \\ 0 & \text{otherwise} \end{cases}, \tag{7}$$

where θ_{11} and θ_{12} are the irradiation angles of the LED and the reflection area, respectively, ϕ_{11} and ϕ_{12} are the incident angles of the reflection area and the PD, respectively, d_{11} is the distance between the LED and the reflection area and d_{12} is the distance between the reflection area and the PD, ρ is the reflection coefficient, and $\mathrm{d}A_{\text{ref}}$ is the acreage of the reflection area.

Then, the received optical power P_r can be obtained by $P_r = R_{\text{PD}} P_t \left[H_L(0) + \int_{A_{\text{ref}}} \mathrm{d}H_N(0) \right]$ with the optical radiation power being P_t. Then the electrical power received by the PD can

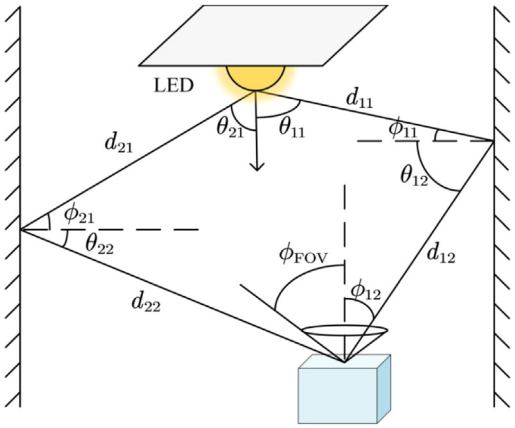

Fig. 3. The NLOS propagation of visible light with first reflection considered.

be similarly described as

$$P_{\mathrm{ele}} = \left\{ R_{\mathrm{PD}} P_t \left[H_L(0) + \int_{A_{\mathrm{ref}}} \mathrm{d}H_N(0) \right] \right\}^2 + \sigma_n^2. \tag{8}$$

3.3. Unified position representation for different receiver orientation via coordinate rotation

For most existing works regarding indoor localization, the receive plane, i.e., the PD of the user terminal is usually assumed to be parallel to the transmit plane, i.e., the ceiling. In this case, the PD can communicate with the LEDs via the LOS link propagation. However, it cannot be guaranteed that the orientation of the user terminal is always perpendicular to the transmit plane, especially in realistic complex scenarios. Therefore, it is necessary to consider the common case of different orientation angles of the user terminal, which leads to a 4D situation including the 3D spatial location and the orientation. In this case, the user terminal can rotate with random orientation, and then the LOS link between the PD and some of the LEDs might be blocked.

As we all know, the rotation of the user terminal also has three degrees-of-freedom of three orientations in the 3D localization system. In the given Cartesian coordinate system as illustrated in Fig. 1, according to the Euler's rotation theorem, the location coordinates of the user terminal will change after a rotation operation with the rotation angle of α, β, γ around the x, y, z axes, and the new coordinates can be represented using the rotation matrix as given by

$$R_x = \begin{bmatrix} 1 & 0 & 0 \\ 0 & \cos(\alpha) & -\sin(\alpha) \\ 0 & \sin(\alpha) & \cos(\alpha) \end{bmatrix} \quad R_y = \begin{bmatrix} \cos(\beta) & 0 & \sin(\beta) \\ 0 & 1 & 0 \\ -\sin(\beta) & 0 & \cos(\beta) \end{bmatrix}$$
$$R_z = \begin{bmatrix} \cos(\gamma) & -\sin(\gamma) & 0 \\ \sin(\gamma) & \cos(\gamma) & 0 \\ 0 & 0 & 1 \end{bmatrix}. \tag{9}$$

4. Four-dimensional indoor visible light positioning enabled by deep learning

4.1. Four-dimensional visible light positioning framework

First, we assume a special case where the PD of the user terminal remains to be parallel to the transmit plane, and then we extend the model to fit the general case with different orientation. The user terminal can move randomly in a 3D space inside the room. The coordinates of the LEDs and the mobile user terminal are represented by the established coordinate system as defined in Section 3.1. We first consider the visible light channel with only LOS propagation, and then we take NLOS propagation into consideration. For the LOS-only channel, we denote the coordinate vector of the PD at the ith as $\boldsymbol{p}_i$ and the coordinate vector of the jth LED as $\boldsymbol{l}_j$. Then, the distance vector from the ith PD to the jth LED is $\boldsymbol{d}_{i,j} = \boldsymbol{l}_j - \boldsymbol{p}_i$. According to the LOS channel model given by Eq. (2) in Section 3, the cosine values of the irradiation angle and the incident angle can be obtained as

$$\cos\left(\theta_{i,j}\right) = -\frac{\boldsymbol{n}_L \cdot \boldsymbol{d}_{i,j}}{\left\|\boldsymbol{d}_{i,j}\right\|_2}, \quad \cos\left(\phi_{i,j}\right) = \frac{\boldsymbol{n}_P \cdot \boldsymbol{d}_{i,j}}{\left\|\boldsymbol{d}_{i,j}\right\|_2}, \tag{10}$$

where $\boldsymbol{n}_P$ is the unit vector of the PD and $\boldsymbol{n}_L$ is the unit vector of the LED. Then the received electrical power is regarded as the RSS.

In order to investigate the influence of the NLOS propagation on the positioning performance, the first reflection of the visible light from the walls, which contributes most of the energy of the NLOS channel [2], is taken into consideration. The wall can be partitioned into a number of small reflection areas with a specific center coordinate represented in the given coordinate system. According to the NLOS channel model given by Eq. (7) in Section 3, all the cosine values of the irradiation angles of each LED and each reflection area, the cosine values of the incident angles of each reflection area and the PD, the distance between each LED and each reflection area, and the distance between each reflection area and the PD, can be calculated. In this case, the NLOS information can be contained in the received RSS.

In fact, using a mobile user terminal as the receiver, it is unrealistic to fix the orientation of the PD. Thus, it is necessary to consider the orientation of the user terminal, which can be regarded as an extra dimension apart from the 3D coordinates, leading to a 4D positioning paradigm. According to the research of the orientation of the indoor receivers [50], the range of the three rotation angles is $\alpha \in [-180^\circ, 180^\circ)$, $\beta \in [-90^\circ, 90^\circ)$ and $\gamma \in [0^\circ, 360^\circ)$, which follows a truncated Laplacian distribution. Based on the Euler's rotation theorem given by Eq. (9) in Section 3, we suppose that the user terminal rotates in the order of z, y, x, and then the coordinate vector and unit vector of the PD at the ith position can be transferred to $\boldsymbol{p}_i R_z R_y R_x$ and $\boldsymbol{n}_P R_z R_y R_x$, respectively. Thus, the DC gain of the VLC channel in Eqs. (2) and (7) after rotation can also be recalculated. At this time, the information of the orientation of the user terminal is embedded in the RSS, which facilitates the deep learning method to find a better mapping between the spatial state data and the location coordinates utilizing this inherent information of orientation.

4.2. Proposed CRNN architecture for four-dimensional VLP

With the improvement of the learning capacity of deep neural networks and the increase of computing power, deep learning can extract more and more abstract features. Classical deep learning models such as DNN, CNN and recurrent neural network (RNN), can be utilized

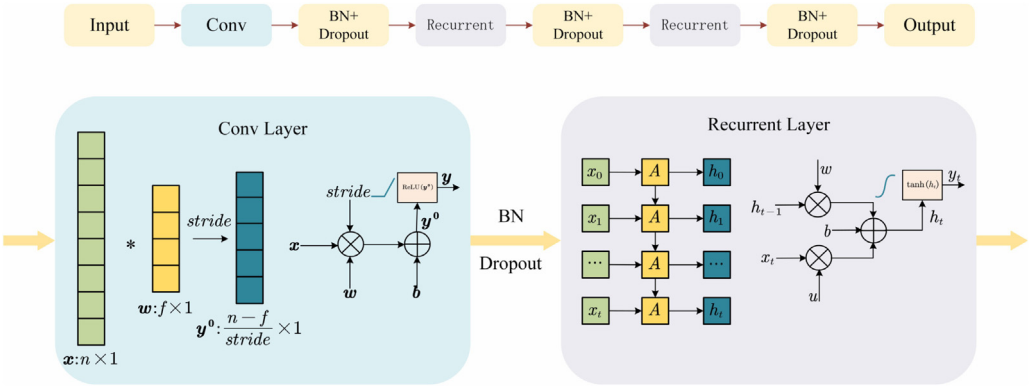

Fig. 4. Structure of the proposed CRNN model utilized for 4D indoor high-precision VLP.

for the task of VLP. In order to deal with the challenge of various orientation of the user terminal and the NLOS propagation of visible light, a hybrid deep learning model, i.e., CRNN, is devised, which can extract the complex geometric information for 4D VLP.

4.2.1. Classical deep learning for VLP

To investigate the performance of deep learning for the task of VLP, classical deep learning models including DNN, CNN, and RNN are applied. First, a DNN consisting of three hidden fully connected layers with 128 neurons is applied. All of neurons are activated by rectified linear units (ReLU), and a linear function is utilized for activation at the output layer. During the training process, the distribution of the input of each layer changes with the parameters from the previous layer, which limits the speed of training. For the CNN, to process the one-dimensional (1D) data of coordinates in localization, three 1D hidden convolutional (Conv) layers are constructed. Each Conv layer contains 32 filters and a convolution kernel with size of 16. The last Conv layer is flattened to a fully connected output layer activated by a linear function. In addition, an RNN consisting of three hidden recurrent layers is constructed for VLP based on the idea of graph expansion and parameters sharing.

4.2.2. CRNN-based four-dimensional VLP (CR4D-VLP)

According to the principle of three classical deep learning models, the fully connected layer can synthesize the extracted features. The Conv layer can share parameters and extract the desired features according to the objective function. The recurrent layer can better utilize the historical data in a sequence. This inspires the idea to fully exploit the advantages of the three models. Thus, a CRNN model is devised, in which a fully connected layer is employed as the output layer, a 1D Conv layer and two recurrent layers are utilized as three hidden layers so that each layer can inherit its own characteristics and share the advantages. Then, the modules of batch normalization (BN) and dropout are employed after each hidden layer to avoid overfitting and improve the generalization ability. The structure of the proposed CRNN model is illustrated in Fig. 4. In the following, the process of the localization data in the proposed method of CR4D-VLP will be described in detail.

Firstly, the input localization data is normalized in the preprocessing stage in order to improve the accuracy and accelerate the convergence speed of the CRNN model. By subtracting its mean and then dividing by the variance of the data, the preprocessed data satisfies a

standard normal distribution with zero mean and variance of one. In addition, by performing normalization on each training batch after each hidden layer, the CRNN model can accelerate the learning rate and reduce the dependence of the gradient on the scale of the parameters. In addition, by randomly *turning off* some neurons, i.e., selecting some neurons that do not participate in the training to prevent their common adaptation, the dropout module employed in the CRNN model can effectively prevent overfitting in the training process.

In the input layer, we reshape the data into size of $n \times 1$ and send the data to the 1D Conv layer. As shown in Fig. 4, the $n \times 1$ data is convoluted with a $f \times 1$ convolution kernel using a fixed stride in the 1D Conv layer. Then a bias b is added on the convolution result and the ReLU is employed for activation. Afterwards, the output of the Conv layer is adjusted using a pooling function that not only suppresses the noise, but also reduces the computational complexity of the model. As for the subsequent recurrent layer, the data is input over t moments, respectively, in the first recurrent layer, and the state output h_t at each moment is calculated according to the shared parameter matrix A and the bias b. Then the hyperbolic tangent function tanh() is applied for activation, and the final output is the entire state sequence. The structure of the second recurrent layer is the same as the first recurrent layer, but the final output is no longer the entire state sequence. In the output layer, the data is activated by a linear function.

Finally, the optimizer is also important for the CRNN training process. The Adam optimizer is employed for training, which is a first-order optimizer that iteratively updates the weights with the training data. For the Adam parameters, the learning rate for updating the weights is set as 0.001, which enforces the optimizer to converge to a better performance. The exponential decay rate of the first-order and the second-order moments is set as 0.9 and 0.999, respectively. The history information of the second-order gradients is not preserved during the training process.

For the task of indoor VLP in this paper, the RSS is taken as the feature data and the coordinates of the user terminal is regarded as the label data, which is utilized to train CRNN model. According to the principle of visible light propagation, when the PD of the user terminal is perpendicular to the transmit plane, deterministic geometric information from all the LEDs on the transmit plane can be obtained via direct LOS propagation links. In this case, the isotropic NLOS links generated by many reflections by the walls might contaminate the geometric information contained in the RSS contributed by the LOS links. Thus, the positioning performance suffers from degradation. However, in the case where the PD is rotating with a random orientation, the geometric information of LOS links from all LEDs can no longer be acquired. In this case, some extra spatial information embedded in the NLOS links can be exploited to compensate for the positioning performance of the deep learning model, which can improve the accuracy of 4D VLP.

4.3. Theoretical analysis for the bound of VLP accuracy

In this subsection, we will derive the theoretical bound of the accuracy of VLP, which can serve as a guidance for experiments and system optimization. For different models and algorithms in positioning, the performance bound can generally be evaluated from three aspects: unbiasedness, validity, and consistency. Generally, the Cramér–Rao lower bound (CRLB), which can be determined by the variance of any unbiased estimator, takes all the three aspects into consideration. Thus, we will investigate the CRLB to evaluate the accuracy of the proposed scheme.

The CRLB has been derived for some localization schemes in literature [2]. Based on the procedure of CRLB derivation in various positioning systems, the CRLB of the RSS-based distance coordinate vector estimation is derived considering direct link propagation without loss of generality. According to Eqs. (2) and (10), assuming that the distance coordinate vector between the PD at the ith position to the jth LED is $\left(a_{i,j}, b_{i,j}, c_{i,j}\right)$, $\boldsymbol{n_i} = (0, 0, 1)$, $\boldsymbol{n_j} = (0, 0, -1)$, respectively, the visible light channel DC gain can be rewritten as

$$H_{i,j} = \frac{(m+1)A_{\mathrm{PD}}c_{i,j}^{m+1}}{2\pi\left(a_{i,j}^2 + b_{i,j}^2 + c_{i,j}^2\right)^{(m+3)/2}} T_s(\phi)g(\phi). \tag{11}$$

Via a specific time-domain or frequency-domain multiple access technique to distinguish the signals sent from different LEDs, the received observations at the user terminal can be expressed as

$$\boldsymbol{y} = R_{\mathrm{PD}}\boldsymbol{H}\boldsymbol{x} + \boldsymbol{n}, \tag{12}$$

where $\boldsymbol{y}$ is the output signal of the PD at each location, $\boldsymbol{x}$ is the transmitted optical power of each LED, $\boldsymbol{H}$ is the channel gain matrix with its entry $H_{i,j}$ as given by Eq. (11), and $\boldsymbol{n}$ is the additive white Gaussian noise with zero mean and variance of σ_n^2. Then the probability density function of $\boldsymbol{y}$ conditioned on $\boldsymbol{d_{i,j}}$ can be expressed as

$$f\left(\boldsymbol{y}|\boldsymbol{d}_{i,j}\right) = \frac{1}{\sqrt{2\pi}\sigma_n} \exp\left\{-\frac{(\boldsymbol{y} - R_{\mathrm{PD}}\boldsymbol{H}\boldsymbol{x})(\boldsymbol{y} - R_{\mathrm{PD}}\boldsymbol{H}\boldsymbol{x})^{\mathrm{T}}}{2\sigma_n^2}\right\}. \tag{13}$$

Therefore, the root mean square error of the distance coordinate vector, which is the CRLB of the positioning method, satisfies

$$\mathrm{RMSE}(a, b, c) \geqslant \sqrt{\mathrm{trace}\left(\mathbf{J}^{-1}\right)}, \tag{14}$$

where $\mathbf{J}$ is the fisher information matrix (FIM), which is given by

$$\mathbf{J} = E\left[(\nabla_d \ln f(\boldsymbol{d}))(\nabla_d \ln f(\boldsymbol{d}))^{\mathrm{T}}\right], \tag{15}$$

where ∇ represents the gradient operator. According to Eqs. (13) and (14), the FIM can be rewritten as

$$\mathbf{J} = \frac{R_{\mathrm{PD}}^2}{\sigma_n^2}\begin{bmatrix} \boldsymbol{x}^{\mathrm{T}}\mathbf{U}^{d_1,d_1}\boldsymbol{x} & \boldsymbol{x}^{\mathrm{T}}\mathbf{U}^{d_1,d_2}\boldsymbol{x} & \boldsymbol{x}^{\mathrm{T}}\mathbf{U}^{d_1,d_3}\boldsymbol{x} \\ \boldsymbol{x}^{\mathrm{T}}\mathbf{U}^{d_2,d_1}\boldsymbol{x} & \boldsymbol{x}^{\mathrm{T}}\mathbf{U}^{d_2,d_2}\boldsymbol{x} & \boldsymbol{x}^{\mathrm{T}}\mathbf{U}^{d_2,d_3}\boldsymbol{x} \\ \boldsymbol{x}^{\mathrm{T}}\mathbf{U}^{d_3,d_1}\boldsymbol{x} & \boldsymbol{x}^{\mathrm{T}}\mathbf{U}^{d_3,d_2}\boldsymbol{x} & \boldsymbol{x}^{\mathrm{T}}\mathbf{U}^{d_3,d_3}\boldsymbol{x} \end{bmatrix}, \tag{16}$$

where $\left(\mathbf{U}^{d_N,d_{N'}}\right)_{j,j'}$, $d_N, d_{N'} \in \left\{a_{i,j}, b_{i,j}, c_{i,j}\right\}$ is defined as

$$\left(\mathbf{U}^{d_N,d_{N'}}\right)_{j,j'} = \left[\left(\frac{\partial}{\partial d_N}\boldsymbol{H}\right)^{\mathrm{T}}\left(\frac{\partial}{\partial d_{N'}}\boldsymbol{H}\right)\right]_{j,j'} = \sum_{i=1}^{M}\frac{\partial}{\partial d_N}H_{i,j}\frac{\partial}{\partial d_{N'}}H_{i,j'}, \tag{17}$$

where the derivatives of the channel gain with respect to d_N and $d_{N'}$ can be represented by

$$\frac{\partial}{\partial a_{i,j}}H_{i,j} = -\frac{a_{i,j}(m+3)(m+1)A_{\mathrm{PD}}c_{i,j}^{m+1}}{2\pi\left(a_{i,j}^2 + b_{i,j}^2 + c_{i,j}^2\right)^{(m+5)/2}} T_s(\phi)g(\phi)$$

Table 1
Simulation parameters.

Parameter	Value
LED field of view	90°
LED half-power angle $\theta_{1/2}$	60°
Wall reflectivity ρ	75%
PD Responsivity R_{PD}	0.65
PD field of view ϕ_{FOV}	70°
Concentrator refractive index n	1.5
PD Effective area A_{PD}	1 cm^2
Optical filter gain $T_s(\phi)$	1

$$\frac{\partial}{\partial b_{i,j}}H_{i,j} = -\frac{b_{i,j}(m+3)(m+1)A_{\mathrm{PD}}c_{i,j}^{m+1}}{2\pi\left(a_{i,j}^2+b_{i,j}^2+c_{i,j}^2\right)^{(m+5)/2}}T_s(\phi)g(\phi)$$
$$\frac{\partial}{\partial c_{i,j}}H_{i,j} = \frac{(m+1)A_{\mathrm{PD}}\left[a_{i,j}^2+b_{i,j}^2+c_{i,j}^2-(m+3)a_{i,j}\right]}{2\pi\left(a_{i,j}^2+b_{i,j}^2+c_{i,j}^2\right)^{(m+5)/2}}T_s(\phi)g(\phi). \tag{18}$$

Remark: In the derivation process of the CRLB of the positioning accuracy, it can be noted intuitively that the positioning accuracy is affected by different factors such as the PD responsivity, noise, Lambertian coefficient, effective area, optical filter gain, and optical concentrator refractive index. In addition to these direct factors, potential factors such as the number of LEDs, the spatial patterns of the deployment of the LEDs, and the room size can also have different effects on the localization accuracy. Hence, we investigate the influence of some of these direct and potential factors on the positioning performance via simulations in the next section.

5. Simulation results and discussions

5.1. Dataset preparation and experimental setup

After the CRNN is formulated, it is worth paying attention to the generation and processing of the dataset which is influential on the performance of deep learning. When generating the dataset, some parameter related to visible light signal transmission are set as shown in Table 1. Next, we will describe the method to generate and process the dataset in detail.

Firstly, 16 LEDs are deployed with equal spacing on the ceiling of a room with its size of 5 m × 5 m × 3 m, in which a 3D rectangular coordinate system is established according to the method shown in Fig. 1, with a corner of the room being the origin point. The coordinates of the 16 LEDs can be known a priori. Then, the user terminal moves randomly in the 3D space with size of 5 m × 5 m × 1.5 m in the room with its PD maintained parallel to the transmit plane, which generates the user position dataset of size 10^5 and the RSS dataset of size $10^5 \times 16$, respectively. The generated RSS dataset has taken both LOS and NLOS propagation links into consideration. Meanwhile, the RSS dataset of size $10^5 \times 16$ for random orientation of the PD can also be generated corresponding to the 4D VLP scenarios. Afterwards, the same procedures are conducted to generate a dataset of order 10^6. To evaluate the effects of some environmental factors on the learning performance, such as the LED spatial pattern and

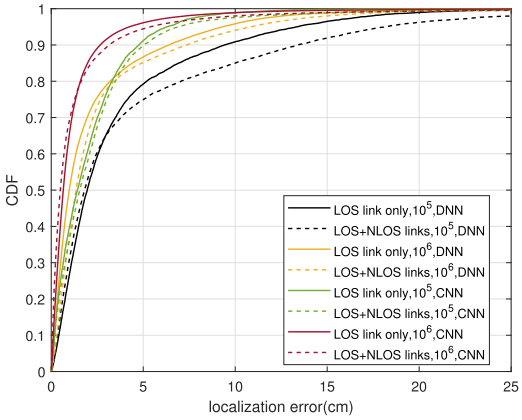

Fig. 5. The CDF of the 3D indoor VLP for the DNN and CNN models in the LOS link only and both LOS and NLOS links scenarios.

room size, some specific datasets related to specific environments are also generated. Each dataset is divided into training set, prediction set and test set with the ratio of $8:1:1$.

In order to analyze the results, the CRNN model and the other three models are trained and then tested. The estimated coordinates are obtained by the trained models, and the positioning error is calculated using the ground-truth coordinates in the test set. The error cumulative distribution function (CDF) is adopted to demonstrate the positioning performance more intuitively.

5.2. Performance evaluation of 3D and 4D visible light positioning

Firstly, we examine the effects of LOS and NLOS propagation and the size of the dataset on the accuracy of indoor 3D positioning for two classical deep-learning-based neural networks, i.e., DNN and CNN, while the PD maintains parallel to the transmit plane. The CDF of the positioning error is shown in Fig. 5. The results indicate that the positioning accuracy can reach centimeter level. The best performance is achieved by the CNN model with only LOS link trained by the dataset of size 10^6, which reaches a positioning error of about 2.67 cm at 90% probability. The worst performance occurs at the DNN model with both LOS and NLOS links trained by the dataset of size 10^5, which has a positioning error of about 13.45 cm at 90% probability. It is observed that the dataset of size 10^6 performs better than the dataset of size 10^5, because within a certain range of the training data amount, the larger the amount of training data, the better the testing generalization performance. At the same time, larger dataset also increases the training complexity. It is also noted that the localization error of the CNN model is smaller than that of the DNN model. The inclusion of NLOS links brings some certain degree of impact on the positioning performance, which verifies that the model can learn deterministic geometric information from all the LEDs via the LOS link, while the inclusion of NLOS links disturbs the explicit geometric information mapping to the coordinates. The results also indicates that other approaches can be applied to mitigate the impact of the inclusion of NLOS links, such as using CNN model in this case.

Next, we further investigate the 4D VLP scenario in which the PD can rotate randomly to have different orientations. The performance of the RNN and the proposed CRNN models are

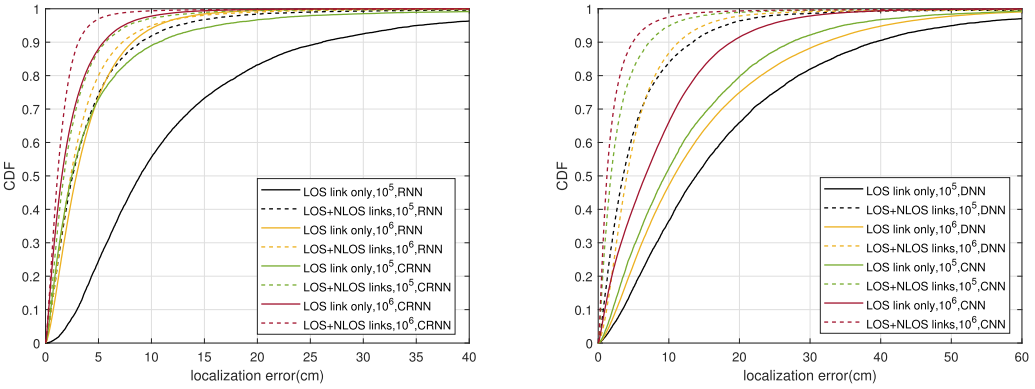

(a) RNN and CRNN (b) DNN and CNN

Fig. 6. The CDF of the localization error of DNN, CNN, RNN and CRNN models for the indoor 4D VLP.

evaluated. The CDF of the positioning error for the RNN and the CRNN models is shown in Fig. 6(a). The CDF of the localization error for the DNN and CNN models is also shown in Fig. 6(b) for comparison. It can be observed from the results that, the inclusion of NLOS links improves the positioning performance. This is because when the PD rotates to a different orientation, the additional NLOS information included in the RSS can compensate for the loss of the geometric information in the LOS links due to blockage, shading, or obscuring. In this case, more favorable geometric information has been fed to the learning model to improve the accuracy of mapping between the RSS and the coordinates.

In addition, the positioning error of the DNN model is still relatively the largest, while the positioning performance from the CNN and RNN models is not much different from each other. It can be observed that the proposed CRNN model performs the best, which verifies that all the merits of the other three models have been exploited. Specifically, the best performance is achieved by the CRNN model with both LOS and NLOS links trained by the dataset of size 10^6, which reaches a positioning error of about 3.12 cm at 90% probability. The worst performance occurs at the DNN model with only LOS link trained by the dataset of size 10^5, which has a positioning error of about 39.44 cm at 90% probability. From these results it is demonstrated that, although the indoor positioning error of the 4D scenario is larger than that of the 3D scenario, it is beyond expectation that the inclusion of NLOS links can reduce the positioning error by contributing to the implicit geometric information conveyed in the RSS. Moreover, the 4D VLP scenario is much more in line with the realistic complex situation because of the flexibility of user orientation.

Furthermore, we examine the average localization error of the DNN, RNN and the proposed CRNN models with respect to the SNR in the 4D VLP scenario, which is shown in Fig. 7. Fig. 7(a) reports the positioning error with the dataset of size 10^5 and Fig. 7(b) provides the results with the dataset of size 10^6. It can be noted from the results that the NLOS links can also improve the performance to a certain extent, which is basically consistent with the results in Fig. 6. With the dataset of size 10^6, the localization error decreases by about 2 cm on average compared to that with the dataset of size 10^5. Besides, it is implied that the proposed CRNN model has an outstanding anti-noise ability at the low SNR region regardless of the dataset size. Compared with the CRNN model, the RNN model is more sensitive to SNR and

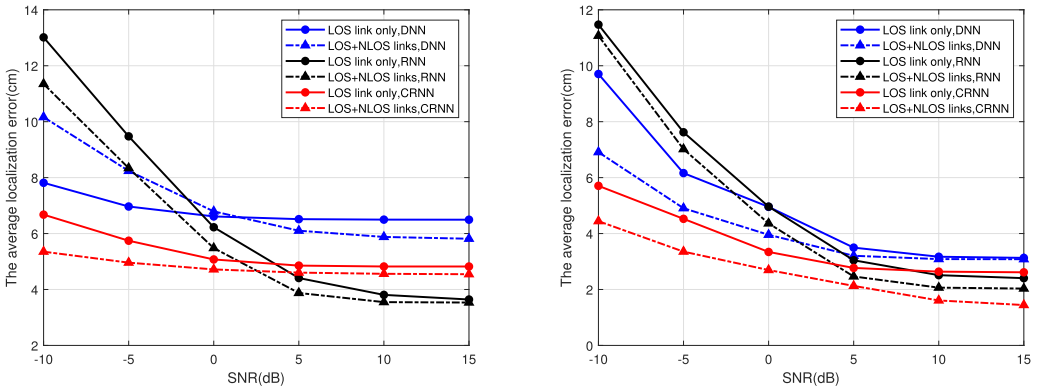

(a) Dataset of size 10^5 (b) Dataset of size 10^6

Fig. 7. The average localization error of the DNN, RNN and CRNN models with respect to SNR for 4D VLP scenario.

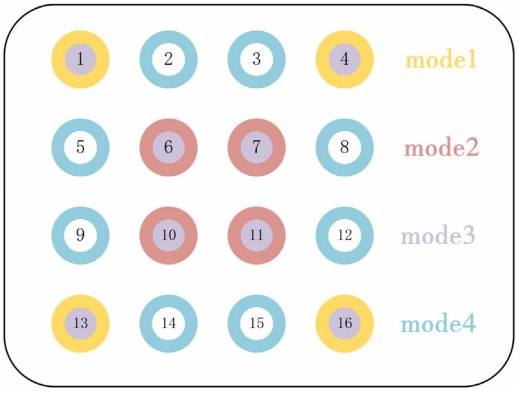

Fig. 8. The spatial patterns of four typical LED deployment modes on the ceiling in the room.

it performs the worst at low SNR. The overall performance of the DNN models is poor over all range of SNR.

5.3. Performance evaluation of environmental factors

In addition to some of the visible light propagation channel and dataset factors influencing positioning performance studied above, next we investigate the influence of some environmental factors, such as the spatial patterns of the LEDs and the room size, on the positioning accuracy. The 16 LEDs on the ceiling can formulate different spatial patterns in various deployment, in which four typical LED deployment modes are investigated, as depicted in Fig. 8. Mode 1 adopts four LEDs in the corner and Mode 2 only employs the central four LEDs. Mode 3 combines the 8 LEDs of Mode 1 and 2, while Mode 4 is the exact opposite of Mode 3. Using the proposed CRNN model, we conduct a comparison experiment of the four LED deployment modes, with positioning dataset of size generated with different PD orientations. The CDF of the localization error is reported in Fig. 9. It can be observed from

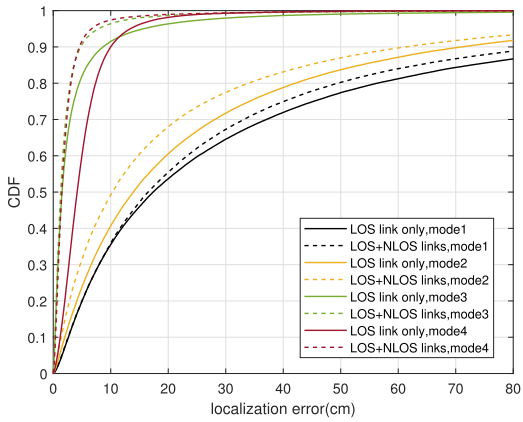

Fig. 9. The CDF of localization error for the indoor 4D VLP with different spatial patterns of LED deployment.

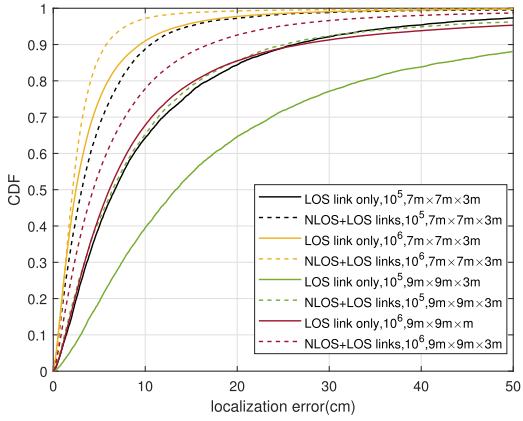

Fig. 10. The CDF of localization error for the indoor 4D VLP in different rooms with different room sizes.

the results that, the number of LEDs deployed is the dominant factor affecting the positioning accuracy. When the number of LEDs is the same, a more concentrated spatial pattern of the LEDs deployment can achieve a better performance. The best performance of positioning error achieved is about 4.58 cm at 90% probability when NLOS links are exploited for the 4D VLP scenario.

In addition, we evaluate the positioning performance of the proposed CRNN model for the 4D VLP task using dataset of size 10^5 and 10^6 generated in two rooms of different room sizes, i.e., 7 m $\times$ 7 m $\times$ 3 m and 9 m $\times$ 9 m $\times$ 3 m, respectively. The CDF of the positioning error is depicted in Fig. 10. It can be observed that, the scheme with both LOS and NLOS links outperforms that with the LOS only link. Since the deployment of LEDs is more scattered when the room is larger with the same number of LEDs, the positioning error thus increases.

Finally, we examine the localization error of the proposed CRNN model in different room sizes with respect to SNR using dataset of size 10^5. From Fig. 11, it is shown that the inclusion of NLOS links can make up for some performance loss, and the anti-noise ability of the CRNN model is effective at low SNR region. Specifically, in the room of size 7 m $\times$ 7 m $\times$ 3 m, the

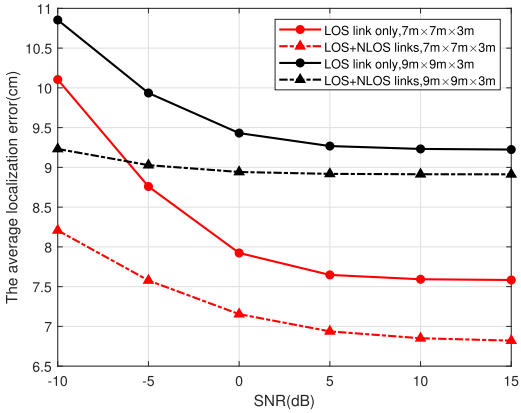

Fig. 11. The average localization error of the CRNN model over different room sizes with respect to SNR.

average localization error of 4D VLP is about 6.82 cm at the SNR of 15 dB with both LOS and NLOS links considered. In the room of size 9 m × 9 m × 3 m, the average localization error is about 8.91 cm at the SNR of 15 dB with both LOS and NLOS links.

6. Conclusion

In this work, an indoor CR4D-VLP framework has been established, where the so-called 4D is to take the user terminal orientation into account as an extension to the original 3D spatial location to deal with more realistic and complex indoor localization scenarios. The LOS and NLOS propagation links have been investigated, by which an interesting phenomenon has been discovered. That is, the inclusion of NLOS links has a detrimental impact on the positioning error when the PD maintains parallel to the transmit plane. However, when the PD rotates to a random orientation, considering the NLOS links can compensate for the localization performance loss of the LOS only link thanks to the implicit geometric information extracted from NLOS links by the proposed CRNN model. The proposed CRNN model has combined the advantages of three types of classical deep learning models, which has satisfactory anti-noise ability especially at the low SNR region. Moreover, we have examined the influence of some important environmental factors, such as the spatial patterns of LED deployment and room sizes, on the localization accuracy. The simulation results have demonstrated that the proposed CR4D-VLP scheme significantly improves the indoor positioning accuracy compared to existing benchmarks by effectively utilizing the available indoor LED resources. It is promising to apply the proposed visible light localization technology to more complex and different types of scenarios with various patterns of LED deployments and complicated channel characteristics.

Declaration of Competing Interest

The authors declare that they have no known competing financial interests or personal relationships that could have appeared to influence the work reported in this paper.

CRediT authorship contribution statement

Danping Su: Conceptualization, Formal analysis, Investigation, Methodology, Software. **Xianyao Wang:** Data curation, Validation, Writing – original draft. **Sicong Liu:** Conceptualization, Methodology, Writing – review & editing. **Wenbo Ding:** Project administration, Writing – review & editing.

Acknowledgments

This work is supported in part by the National Natural Science Foundation of China under grant 61901403, in part by the Science and Technology Key Project of Fujian Province, China (Nos. 2021HZ021004 and 2019HZ020009), in part by the open research fund of National Mobile Communications Research Laboratory, Southeast University (No. 2023D10), in part by the Youth Innovation Fund of Natural Science Foundation of Xiamen (No. 3502Z20206039), in part by the Science and Technology Key Project of Xiamen under Grant 3502Z20221027, and in part by the Xiamen Special Fund for Marine and Fishery Development under Grant 21CZB011HJ02.

References

[1] M. Garcia Puyol, D. Bobkov, P. Robertson, T. Jost, Pedestrian simultaneous localization and mapping in multistory buildings using inertial sensors, IEEE Trans. Intell. Transp. Syst. 15 (4) (2014) 1714–1727, doi:10.1109/TITS.2014.2303115.

[2] Y. Zhuang, L. Hua, L. Qi, J. Yang, P. Cao, Y. Cao, Y. Wu, J. Thompson, H. Haas, A survey of positioning systems using visible LED lights, IEEE Commun. Surv. Tutor. 20 (3) (2018) 1963–1988, doi:10.1109/COMST.2018.2806558.

[3] C. Chen, Y. Chen, Y. Han, H.-Q. Lai, K.J.R. Liu, Achieving centimeter-accuracy indoor localization on WiFi platforms: a frequency hopping approach, IEEE Internet Things J. 4 (1) (2017) 111–121, doi:10.1109/JIOT.2016.2628701.

[4] Y. Ma, C. Tian, Y. Jiang, A multitag cooperative localization algorithm based on weighted multidimensional scaling for passive UHF RFID, IEEE Internet Things J. 6 (4) (2019) 6548–6555, doi:10.1109/JIOT.2019.2907771.

[5] N. Yu, X. Zhan, S. Zhao, Y. Wu, R. Feng, A precise dead reckoning algorithm based on bluetooth and multiple sensors, IEEE Internet Things J. 5 (1) (2018) 336–351, doi:10.1109/JIOT.2017.2784386.

[6] Y. Xu, Y.S. Shmaliy, C.K. Ahn, T. Shen, Y. Zhuang, Tightly coupled integration of INS and UWB using fixed-lag extended UFIR smoothing for quadrotor localization, IEEE Internet Things J. 8 (3) (2021) 1716–1727, doi:10.1109/JIOT.2020.3015351.

[7] J. Song, T. Cao, H. Zhang, Performance analysis of a low-complexity nonorthogonal multiple access scheme in visible light communication downlinks using pulse modulations, Intell. Converg. Netw. 2 (1) (2021) 50–65, doi:10.23919/ICN.2020.0024.

[8] Y. Zhang, H. Zhang, J. Cosmas, N. Jawad, K. Ali, B. Meunier, A. Kapovits, L.-K. Huang, W. Li, L. Shi, X. Zhang, J. Wang, I. Koffman, M. Robert, C.C. Zarakovitis, Internet of radio and light: 5G building network radio and edge architecture, Intell. Converg. Netw. 1 (1) (2020) 37–57, doi:10.23919/ICN.2020.0002.

[9] L. Xiao, G. Sheng, S. Liu, H. Dai, M. Peng, J. Song, Deep reinforcement learning-enabled secure visible light communication against eavesdropping, IEEE Trans. Commun. 67 (10) (2019) 6994–7005, doi:10.1109/TCOMM.2019.2930247.

[10] F. Yang, J. Gao, S. Liu, Priori aided compressed sensing-based clipping noise cancellation for ACO-OFDM systems, IEEE Photonics Technol. Lett. 28 (19) (2016) 2082–2085, doi:10.1109/LPT.2016.2585224.

[11] J. Luo, L. Fan, H. Li, Indoor positioning systems based on visible light communication: state of the art, IEEE Commun. Surv. Tutor. 19 (4) (2017) 2871–2893, doi:10.1109/COMST.2017.2743228.

[12] S. Tomic, M. Beko, R. Dinis, RSS-based localization in wireless sensor networks using convex relaxation: noncooperative and cooperative schemes, IEEE Trans. Veh. Technol. 64 (5) (2015) 2037–2050, doi:10.1109/TVT.2014.2334397.

[13] N. BniLam, D. Joosens, M. Aernouts, J. Steckel, M. Weyn, LoRay: AoA estimation system for long range communication networks, IEEE Trans. Wirel. Commun. 20 (3) (2021) 2005–2018, doi:10.1109/TWC.2020.3038565.
[14] W. Li, Y. Jia, J. Du, TOA-based cooperative localization for mobile stations with NLOS mitigation, J. Frankl. Inst. 353 (6) (2016) 1297–1312, doi:10.1016/j.jfranklin.2016.02.004.
[15] G. Wang, S. Cai, Y. Li, N. Ansari, A bias-reduced nonlinear WLS method for TDOA/FDOA-based source localization, IEEE Trans. Veh. Technol. 65 (10) (2016) 8603–8615, doi:10.1109/TVT.2015.2508501.
[16] Z. Zheng, H. Zhang, W.-Q. Wang, H.C. So, Source localization using TDOA and FDOA measurements based on semidefinite programming and reformulation linearization, J. Frankl. Inst. 356 (18) (2019) 11817–11838, doi:10.1016/j.jfranklin.2019.10.029.
[17] L. Gui, F. Xiao, Y. Zhou, F. Shu, T. Val, Connectivity based DV-hop localization for internet of things, IEEE Trans. Veh. Technol. 69 (8) (2020) 8949–8958, doi:10.1109/TVT.2020.2998093.
[18] M.T. Hoang, Y. Zhu, B. Yuen, T. Reese, X. Dong, T. Lu, R. Westendorp, M. Xie, A soft range limited k-nearest neighbors algorithm for indoor localization enhancement, IEEE Sens. J. 18 (24) (2018) 10208–10216, doi:10.1109/JSEN.2018.2874453.
[19] T. Lan, X. Wang, Z. Chen, J. Zhu, S. Zhang, Fingerprint augment based on super-resolution for WiFi fingerprint based indoor localization, IEEE Sens. J. 22 (12) (2022) 12152–12162, doi:10.1109/JSEN.2022.3174600.
[20] X. Sun, Y. Zhuang, J. Huai, L. Hua, D. Chen, Y. Li, Y. Cao, R. Chen, RSS-based visible light positioning using nonlinear optimization, IEEE Internet Things J. 9 (15) (2022) 14137–14150, doi:10.1109/JIOT.2022.3156616.
[21] H. Steendam, A 3-D positioning algorithm for AOA-based VLP with an aperture-based receiver, IEEE J. Sel. Areas Commun. 36 (1) (2018) 23–33, doi:10.1109/JSAC.2017.2774478.
[22] S.-Y. Jung, S. Hann, C.-S. Park, TDOA-based optical wireless indoor localization using LED ceiling lamps, IEEE Trans. Consum. Electron. 57 (4) (2011) 1592–1597, doi:10.1109/TCE.2011.6131130.
[23] P. Du, S. Zhang, C. Chen, A. Alphones, W.-D. Zhong, Demonstration of a low-complexity indoor visible light positioning system using an enhanced TDOA scheme, IEEE Photonics J. 10 (4) (2018) 1–10, doi:10.1109/JPHOT.2018.2841831.
[24] Y.-A. Chen, Y.-T. Chang, Y.-C. Tseng, W.-T. Chen, A framework for simultaneous message broadcasting using CDMA-based visible light communications, IEEE Sens. J. 15 (12) (2015) 6819–6827, doi:10.1109/JSEN.2015.2463684.
[25] S.-H. Yang, H.-S. Kim, Y.-H. Son, S.-K. Han, Three-dimensional visible light indoor localization using AOA and RSS with multiple optical receivers, J. Lightwave Technol. 32 (14) (2014) 2480–2485, doi:10.1109/JLT.2014.2327623.
[26] B. Zhu, J. Cheng, Y. Wang, J. Yan, J. Wang, Three-dimensional VLC positioning based on angle difference of arrival with arbitrary tilting angle of receiver, IEEE J. Sel. Areas Commun. 36 (1) (2018) 8–22, doi:10.1109/JSAC.2017.2774435.
[27] A. Sahin, Y.S. Eroglu, I. Guvenc, N. Pala, M. Yuksel, Hybrid 3-D localization for visible light communication systems, J. Lightwave Technol. 33 (22) (2015) 4589–4599, doi:10.1109/JLT.2015.2477502.
[28] I. Goodfellow, Y. Bengio, A. Courville, Deep Learning, MIT Press, 2016. http://www.deeplearningbook.org
[29] B. Hartpence, A. Kwasinski, CNN and MLP neural network ensembles for packet classification and adversary defense, Intell. Converg. Netw. 2 (1) (2021) 66–82, doi:10.23919/ICN.2020.0023.
[30] G. Bayar, G. Hambarci, Improving measurement accuracy of indoor positioning system of a Mecanum wheeled mobile robot using Monte Carlo - Latin hypercube sampling based machine learning algorithm, J. Frankl. Inst. (2022), doi:10.1016/j.jfranklin.2022.07.037.
[31] T. Wei, S. Liu, X. Du, Visible light integrated positioning and communication: a multi-task federated learning framework, IEEE Trans. Mob. Comput. (2022) 1–18, doi:10.1109/TMC.2022.3207164.
[32] D. Su, X. Liu, S. Liu, Three-Dimensional Indoor Visible Light Localization: A Learning-Based Approach, UbiComp '21, Association for Computing Machinery, New York, NY, USA, 2021, pp. 672–677, doi:10.1145/3460418.3480406.
[33] M. Min, W. Wang, L. Xiao, Y. Xiao, Z. Han, Reinforcement learning-based sensitive semantic location privacy protection for VANETs, China Commun. 18 (6) (2021) 244–260, doi:10.23919/JCC.2021.06.019.
[34] H. Zhang, J. Cui, L. Feng, A. Yang, H. Lv, B. Lin, H. Huang, High-precision indoor visible light positioning using deep neural network based on the Bayesian regularization with sparse training point, IEEE Photonics J. 11 (3) (2019) 1–10, doi:10.1109/JPHOT.2019.2912156.
[35] K. Majeed, S. Hranilovic, Passive indoor visible light positioning system using deep learning, IEEE Internet Things J. 8 (19) (2021) 14810–14821, doi:10.1109/JIOT.2021.3072201.

[36] A.H.A. Bakar, T. Glass, H.Y. Tee, F. Alam, M. Legg, Accurate visible light positioning using multiple-photodiode receiver and machine learning, IEEE Trans. Instrum. Meas. 70 (2021) 1–12, doi:10.1109/TIM.2020.3024526.
[37] P. Wang, B. Guo, Z. Wang, Z. Yu, ShopSense: customer localization in multi-person scenario with passive RFID tags, IEEE Trans. Mob. Comput. 21 (5) (2022) 1812–1828, doi:10.1109/TMC.2020.3029833.
[38] W. Sun, M. Xue, H. Yu, H. Tang, A. Lin, Augmentation of fingerprints for indoor WiFilocalization based on Gaussian process regression, IEEE Trans. Veh. Technol. 67 (11) (2018) 10896–10905, doi:10.1109/TVT.2018.2870160.
[39] B. Hanssens, D. Plets, E. Tanghe, C. Oestges, D.P. Gaillot, M. Liénard, T. Li, H. Steendam, L. Martens, W. Joseph, An indoor variance-based localization technique utilizing the UWB estimation of geometrical propagation parameters, IEEE Trans. Antennas Propag. 66 (5) (2018) 2522–2533, doi:10.1109/TAP.2018.2810340.
[40] Q. Zhu, Q. Xiong, K. Wang, W. Lu, T. Liu, Accurate WiFi-based indoor localization by using fuzzy classifier and MLPs ensemble in complex environment, J. Frankl. Inst. 357 (3) (2020) 1420–1436, doi:10.1016/j.jfranklin.2019.10.028.
[41] H. Huang, A. Yang, L. Feng, G. Ni, P. Guo, Artificial neural-network-based visible light positioning algorithm with a diffuse optical channel, Chin. Opt. Lett. 15 (5) (2017) 050601. http://opg.optica.org/col/abstract.cfm?URI=col-15-5-050601
[42] X. Guo, S. Shao, N. Ansari, A. Khreishah, Indoor localization using visible light via fusion of multiple classifiers, IEEE Photonics J. 9 (6) (2017) 1–16, doi:10.1109/JPHOT.2017.2767576.
[43] R. Liu, Z. Liang, K. Yang, W. Li, Machine learning based visible light indoor positioning with single-LED and single rotatable photo detector, IEEE Photonics J. 14 (3) (2022) 1–11, doi:10.1109/JPHOT.2022.3163415.
[44] C.-Y. Hong, Y.-C. Wu, Y. Liu, C.-W. Chow, C.-H. Yeh, K.-L. Hsu, D.-C. Lin, X.-L. Liao, K.-H. Lin, Y.-Y. Chen, Angle-of-arrival (AOA) visible light positioning (VLP) system using solar cells with third-order regression and ridge regression algorithms, IEEE Photonics J. 12 (3) (2020) 1–5, doi:10.1109/JPHOT.2020.2993031.
[45] T. Yuan, Y. Xu, Y. Wang, P. Han, J. Chen, A tilt receiver correction method for visible light positioning using machine learning method, IEEE Photonics J. 10 (6) (2018) 1–12, doi:10.1109/JPHOT.2018.2880872.
[46] X. Lin, L. Zhang, Intelligent and practical deep learning aided positioning design for visible light communication receivers, IEEE Commun. Lett. 24 (3) (2020) 577–580, doi:10.1109/LCOMM.2019.2958629.
[47] L.-S. Hsu, D.-C. Tsai, C.-W. Chow, Y. Liu, Y.-H. Chang, Y.-Z. Lin, C.-H. Yeh, Y.-C. Wang, Y.-Y. Chen, Using data pre-processing and convolutional neural network (CNN) to mitigate light deficient regions in visible light positioning (VLP) systems, J. Lightwave Technol. 40 (17) (2022) 5894–5900, doi:10.1109/JLT.2022.3184931.
[48] D.-C. Lin, C.-W. Chow, C.-W. Peng, T.-Y. Hung, Y.-H. Chang, S.-H. Song, Y.-S. Lin, Y. Liu, K.-H. Lin, Positioning unit cell model duplication with residual concatenation neural network (RCNN) and transfer learning for visible light positioning (VLP), J. Lightwave Technol. 39 (20) (2021) 6366–6372, doi:10.1109/JLT.2021.3103707.
[49] P.A. Hoeher, 3 - VLC and IR/UV channel modeling, in: P.A. Hoeher (Ed.), Visible Light Communications, Hanser, 2019, pp. 41–64, doi:10.3139/9783446461727.003.
[50] M.A. Arfaoui, M.D. Soltani, I. Tavakkolnia, A. Ghrayeb, C.M. Assi, M. Safari, H. Haas, Invoking deep learning for joint estimation of indoor LiFi user position and orientation, IEEE J. Sel. Areas Commun. 39 (9) (2021) 2890–2905, doi:10.1109/JSAC.2021.3064637.